IEEE Access
Multidisciplinary | Rapid Review | Open Access Journal

Received September 22, 2019, accepted October 19, 2019, date of publication November 7, 2019,
date of current version November 18, 2019.

Digital Object Identifier 10.1109/ACCESS.2019.2951943

A Data-Driven Based Framework of Model Optimization and Neural Network Modeling for Microbial Fuel Cells

FENGYING MA[1], YANKAI YIN[1], SHAOPENG PANG[1], JIAXUN LIU[1], AND WEI CHEN[2,3,4,5], (Member, IEEE)

[1]School of Electrical Engineering and Automation, Qilu University of Technology, Jinan 250353, China
[2]School of Computer Science and Technology, China University of Mining and Technology, Xuzhou 221116, China
[3]Mine Digitization Engineering Research Center of the Ministry of Education, China University of Mining and Technology, Xuzhou 221116, China
[4]Information Engineering College, Beijing Institute of Petrochemical Technology, Beijing 102617, China
[5]School of Earth and Space Sciences, Peking University, Beijing 100871, China

Corresponding author: Wei Chen (chenwdavior@163.com)

This work was supported in part by the National Natural Science Foundation of China under Grant 51874300, in part by the National Natural Science Foundation of China and Shanxi Provincial People's Government Jointly Funded Project of China for Coal Base and Low Carbon under Grant U1510115, in part by the Key Research and Development Program of Shandong Province under Grant 2018GGX103054 and Grant 2017GSF220005, in part by the Open Fund Project of Key Laboratory of Pulp and Paper Science and Technology of Ministry of Education under Grant KF201418, and in part by the Open Research Fund of Key Laboratory of Wireless Sensor Network and Communication, Shanghai Institute of Microsystem and Information Technology, Chinese Academy of Sciences, under Grant 20190902 and Grant 20190913.

ABSTRACT Microbial fuel cells (MFCs) are devices that transform organic matters in wastewater into green energy. Microbial fuel cells systems have strong nonlinearity and high coupling, which involves control science, microbiology, electrochemistry and other disciplines. According to the requirements of microbial fuel cell system for model robustness and accuracy, we designed a comprehensive model optimization framework. Firstly, the influence of uncertain parameters on system was analyzed by combining global sensitivity analysis with uncertainty analysis. In accordance with analysis results, the uncertain parameters were optimized. Secondly, based on the optimized stochastic model, a simplified model was proposed by combining variable selection with neural networks. The results shown that the proposed framework can deeply analysis the influence of uncertain parameters on output, and provide theoretical basis for experimental research. It fully simplifies the original MFCs model, and has guiding significance for other types of fuel cells.

INDEX TERMS Microbial fuel cells, model optimization, variable selection, neural networks.

I. INTRODUCTION

Microbial Fuel Cells (MFCs) which required in lots of field [1]–[3] have received a widespread concern in the past several years as a green energy. MFCs can be considered as equipment realizes a conversion of bioenergy to green energy, taking the organism as the fuel and direct generation of electricity by microbial redox reactions. Many efforts have been directed to the power generation principle and application of MFCs [4]–[6]. The basic reaction principle is that the bacteria oxidize the substrate in the anaerobic anode through a catalyst, and the electrons generated by the anode chamber are transported to the aerobic cathode through an external circuit and form water molecules. Compared with hydrogen oxygen fuel cells and other chemical cells, MFCs use organisms as biocatalysts and possesses the advantages of high resource-using rate, less pollution and mild reaction conditions. However, there are several obstacles constrain the development of MFCs. The main disadvantage of MFCs operation compared to other renewable energy, such as geothermal energy, tidal energy, nuclear power is the low power output, which limits the ability to drive high power devices.

Over the past few years, the main direction of research was microbial cultivation, substrate analysis and electrode modification, various systems were built for different types of MFCs [7], [8]. In addition, a large number of experimental

The associate editor coordinating the review of this manuscript and approving it for publication was Yan-Jun Liu.

studies have also found the impact of operational parameters on MFCs performance, such as ionic concentration [9], temperature [10], [11], pH [12], substrate nitrogen concentration [13], [14], and electrode distance [15]. Zou *et al.* [16] built a new-type MFC with anode material is carbon nanotube (CNT) which coated polypyrrole and E. coli as biocatalyst. Ren *et al.* [17] built an MFC with carboxymethylcellulose as substrate and observed the power density reached 153 $\mathrm{mW\,m^{-2}}$. Katz *et al.* [18] found that the increase of ionic concentration will lead to a increase of maximum power density, chemical oxygen demand (COD) removal efficiency and Coulombic efficiency (CE). In accordance with the study of borax buffer, Qiang *et al.* [19] found that the electronic recovery efficiency can be improved by adding appropriate concentration of borax buffer. Although a large number of studies have yielded good results, they also prove that MFCs is a complex system involving a mass of bio-electrochemical coupling reactions, which result in the high coupling characteristics, high time-delaying performance and uncertainty characteristics.

Modeling is an approach to conduct simulation experiments which require complex operation and high cost, and played a key role in MFCs optimization. On the basis of different modeling objectives, the MFCs models can be segmented into the full-cell models which discusses anode and cathode compartment simultaneous, and the half-cell models focusing on a single compartment [20]. Much of work has been focused on the fields related to MFCs modeling. Picioreanu *et al.* [21] developed a computational MFC biofilm model to study the process of the bacteria on the surface of the anode to form biofilms and changes in biofilm thickness. Alavijeh *et al.* [22] presented an equation for the effluent treatment process of MFCs in combination with the diffusion effect of substrate to biofilm and competition in the same substrate. Katuri *et al.* [23] calculated the current density by introducing the basic Butler-Volmer equation, and used the hyperbolic sine function to represent the anode overpotential. Based on the mass balance, the simple expression of the steady state overpotential of the anode was derived. Ou *et al.* [24] proposed a one-dimensional transient model of single chamber MFC without considering the change of the thickness of the cathode biofilm and the concentration distribution in the biofilm area. In 2010, Zeng, *et al.* [25] developed a two-chamber MFC model supposed that both the anode and cathode reactions can be considered as a continuously stirred tank reactor (CSTR). However, most of the models on the report are inherently complex and cannot be reproduced.

With the continuous updating of MFCs modeling method, the contradiction between theory and application appears. The first reason is that the researchers did not fully consider the influence of uncertainty on the model in the modeling process. The models established from the experimental data are usually only suitable for the presentation of current experiment. Secondly, the model are too complicated and there are several systematic errors in the modeling process. Building a mathematical framework include the sensitivity analysis (SA), uncertainty analysis, and neural network modeling is a viable solution for a complex, microbiology-based MFCs system. In this work, the uncertain parameters in the microbial fuel cells was represented as normal probability distribution, and the input parameters was expressed as uniform distribution. Firstly, the uncertain parameters in the model were optimized by sensitivity analysis and uncertainty analysis. Secondly, a new sampling method was used on the known model to obtain the input and output data. Finally, using genetic algorithm to reduce the dimension of independent variables, and the BP neural network model with the highest accuracy was established.

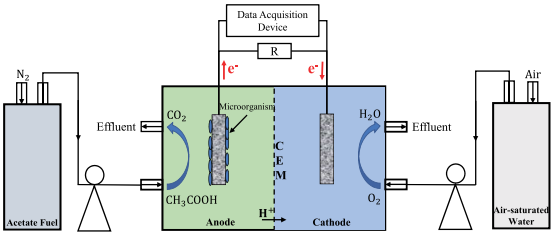

FIGURE 1. Schematic diagram of MFC experiment.

This paper is structured in the following order: Section 2 gives a brief review to the typical continuous flow microbial fuel cell model; Section 3 details the framework for model optimization and neural network modeling presented in this paper; Section 4 shows the results of global sensitivity analysis (GSA) and uncertainty analysis, and based on it, a simplified BP neural network was established.

II. TWO-CHAMBER MICROBIAL FUEL CELL MODEL

A comprehensive differential equation model for the bioreactions and electrochemical phenomena presented in [25] was used as the basis and data source of this research. The basic experimental device is a typical two-chamber microbial fuel cell consisting of cathode chamber and anode chamber separated by a cation-exchange membrane. The schematic diagram is shown in Fig. 1.

Anode chamber ensures anoxic condition by continuously produced nitrogen gas, whereas cathode chamber continuously adds air-saturated water to make the protons react with dissolved oxygen. Both electrodes are made of carbon felt and coated with platinum powder as catalyst. The experimental operation temperature is 30°C and an adjustable resistance is added to the external circuit between the cathode and anode. The modeling includes the Monod-type equation, as is prevalent in modeling of microbial fuel cells and illustrated in subsections below.

Equations of electrochemical reactions occurring at anode and cathode are described as follows:

$$(CH_2O)_2 + 2H_2O \rightarrow 2C_2O + 8H^+ + 3e^-, \quad (1)$$

$$O_2 + 2H_2O + 4e^- \rightarrow 4OH^-. \quad (2)$$

The anode chamber operates under anoxic conditions, and the Monod-type equation was used to describe the anodic

reaction rate. The reaction rate of the anode chamber is given as:

$$r_1 = k_1^0 \exp\left(\frac{\alpha F}{RT}\eta_a\right)\frac{C_{AC}}{K_{AC}+C_{AC}}X, \tag{3}$$

where C_{AC} denotes the concentration of acetate, X is the biomass in the anode compartment, η_a represents the anodic polarization overpotential, K_{AC} is the half velocity rate constant for acetate, α stands for the charge transfer coefficient of the anodic reaction, k_1^0 is the rate constant of the anodic reaction at standard conditions, F represents the Faraday constant, T is the cell operating temperature, and R denote the gas constant.

The Butler-Volmer expression was used to describe the electrochemical reaction, and the reaction rate of the cathode chamber is written as:

$$r_2 = -k_2^0\frac{C_{O_2}}{K_{O_2}+C_{O_2}}\exp\left[(\beta-1)\frac{F}{RT}\eta_c\right], \tag{4}$$

where η_c denotes the overpotential at the cathode, C_{O_2} is the concentration for the dissolved oxygen, β represents the charge transfer coefficient, k_2^0 denotes the rate constant of the cathodic reaction under standard conditions, and K_{O_2} is the half-velocity rate constant for dissolved oxygen.

The anode and cathode chambers of the MFCs system are regarded as a continuous reactor, and four mass balance equations for the acetate, dissolved CO_2, hydrogen ion and biomass in the anode chamber were obtained, respectively, and are defined as follows:

$$V_a\frac{dC_{AC}}{dt} = Q_a\left(C_{AC}^{in}-C_{AC}\right)-A_m r_1, \tag{5}$$

$$V_a\frac{dC_{CO_2}}{dt} = Q_a\left(C_{CO_2}^{in}-C_{CO_2}\right)-2A_m r_1, \tag{6}$$

$$V_a\frac{dC_H}{dt} = Q_a\left(C_H^{in}-C_H\right)+8A_m r_1, \tag{7}$$

$$V_a\frac{dC_X}{dt} = Q_a\left(\frac{X^{in}-X}{f_x}\right)+A_m Y_{ac} r_1 - V_a K_{dec} X, \tag{8}$$

where subscript 'a' and superscript 'in' represent the anode and flow of feed, respectively; V, Q and A_m denote the volume, the flow rate and the cross-section area of membrane, respectively; and Y_{ac}, f_x, K_{dec} denote the bacterial yield, the reciprocal of wash-out fraction and the decay constant for acetate utilizers, respectively.

The same method was used to obtain three mass balance equations for the dissolved O_2, hydroxyls, and M^+ ions in the cathode chamber, respectively, which are written as:

$$V_c\frac{dC_{O_2}}{dt} = Q_c\left(C_{O_2}^{in}-C_{O_2}\right)+A_m r_2, \tag{9}$$

$$V_c\frac{dC_{OH}}{dt} = Q_c\left(C_{OH}^{in}-C_{OH}\right)-4A_m r_2, \tag{10}$$

$$V_c\frac{dC_M}{dt} = Q_c\left(C_M^{in}-C_{O_2}\right)+A_m N_M, \tag{11}$$

where the subscript 'c' means the cathode, N_M stands for the flow of M^+ ions through the membrane, which can be calculated as follows:

$$N_M = \frac{3600 i_{cell}}{F}. \tag{12}$$

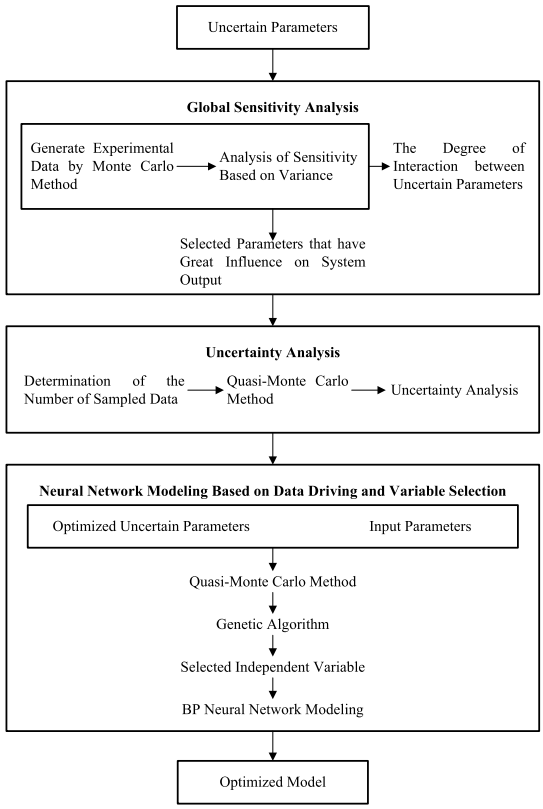

FIGURE 2. Schematic diagram of comprehensive framework.

The charge balances at the anode and cathode are described as follows:

$$C_a\frac{d\eta_a}{dt} = 3600 i_{cell} - 8Fr_1, \tag{13}$$

$$C_c\frac{d\eta_c}{dt} = 3600 i_{cell} + 4Fr_2, \tag{14}$$

where i_{cell} denotes the current density, C_a and C_c stand for the anode capacitance and cathode capacitance, respectively.

The voltage of MFC is expressed as follows:

$$V_{cell} = V_0 - \eta_a + \eta_c - \left(\frac{d^m}{k^m}+\frac{d^{cell}}{k^{aq}}\right)i_{cell}, \tag{15}$$

where V_0 represents the open-circuit voltage, d^m is the membrane thickness, d^{cell} stands for the electrode distance, k^{aq} denotes the conductivity of the solution, and k^m is the conductivity of the membrane.

The description and standard values of the parameters in the model are shown in Table 1.

III. METHODOLOGY

A comprehensive framework for data-driven MFC model analysis and optimization is given in Fig. 2. The framework includes global sensitivity analysis, uncertainty analysis, and neural network modeling based on data driving

TABLE 1. Nominal values of parameters for MFC model.

Description	Symbol/Unit	Value
Flow rate of fuel feed to anode	$Q_{\mathrm{a}}/\mathrm{m}^3\,\mathrm{h}^{-1}$	2.25×10^{-5}
Flow rate feeding to cathode compartment	$Q_{\mathrm{c}}/\mathrm{m}^3\,\mathrm{h}^{-1}$	1.11×10^{-5}
Capacitance of anode	$C_{\mathrm{a}}/\mathrm{F}\,\mathrm{m}^{-2}$	4×10^{2}
Capacitance of cathode	$C_{\mathrm{c}}/\mathrm{F}\,\mathrm{m}^{-2}$	5×10^{2}
Volume of anode compartment	$V_{\mathrm{a}}/\mathrm{m}^3$	5.5×10^{-5}
Volume of cathode compartment	$V_{\mathrm{c}}/\mathrm{m}^3$	5.5×10^{-5}
Concentration of acetate in the influent of anode compartment	$C^{\mathrm{in}}_{\mathrm{AC}}/\mathrm{mol}\,\mathrm{m}^{-3}$	1.56
Concentration of CO_2 in the influent of anode compartment	$C^{\mathrm{in}}_{\mathrm{CO_2}}/\mathrm{mol}\,\mathrm{m}^{-3}$	0
Concentration of bacteria in the influent of anode compartment	$X^{\mathrm{in}}/\mathrm{mol}\,\mathrm{m}^{-3}$	0
Concentration of H^+ in the influent of anode compartment	$C^{\mathrm{in}}_{\mathrm{H}}/\mathrm{mol}\,\mathrm{m}^{-3}$	0
Concentration of dissolved O_2 in the influent of cathode compartment	$C^{\mathrm{in}}_{\mathrm{O_2}}/\mathrm{mol}\,\mathrm{m}^{-3}$	0.3125
Concentration of M^+ in the influent of cathode compartment	$C^{\mathrm{in}}_{\mathrm{M}}/\mathrm{mol}\,\mathrm{m}^{-3}$	0
Concentration of OH^- in the influent of cathode compartment	$C^{\mathrm{in}}_{\mathrm{OH}}/\mathrm{mol}\,\mathrm{m}^{-3}$	0
Faraday's constant	$F/\mathrm{Coulombs}\,\mathrm{mol}^{-1}$	96485.4
Gas constant	$R/\mathrm{J}\,\mathrm{mol}^{-1}\,\mathrm{K}^{-1}$	8.3144
Temperature	T/K	303
Electrical conductivity of membrane	$k^{\mathrm{m}}/\mathrm{Ohm}^{-1}\,\mathrm{m}^{-1}$	17
Thickness of membrane	$d^{\mathrm{m}}/\mathrm{m}$	1.778×10^{-4}
Electrical conductivity of the aqueous solutionn	$k^{\mathrm{aq}}/\mathrm{Ohm}^{-1}\,\mathrm{m}^{-1}$	5
Distance between anode and cathode in the cell	$d^{\mathrm{cell}}/\mathrm{m}$	2.2×10^{-2}
Area of membrane	$A_{\mathrm{m}}/\mathrm{m}^2$	5×10^{-4}
Bacterial yield	$Y_{\mathrm{ac}}/\mathrm{Dimensionless}$	0.05
Decay constant for acetate	$K_{\mathrm{dec}}/\mathrm{h}^{-1}$	8.33×10^{-4}
Reciprocal of wash-out fraction	$f_x/\mathrm{Dimensionless}$	10
Cell open circuit potential	V_0/volt	0.77
Forward rate constant of anode reaction at standard condition	$k^0_1/\mathrm{mol}\,\mathrm{m}^{-2}\,\mathrm{h}^{-1}$	0.207
Forward rate constant of cathode reaction at standard condition	$k^0_2/\mathrm{m}^{12}\,\mathrm{mol}^{-4}\,\mathrm{h}^{-1}$	3.288×10^{-5}
Half velocity rate constant for acetate	$K_{\mathrm{AC}}/\mathrm{mol}\,\mathrm{m}^{-3}$	0.592
Half velocity rate constant for dissolved oxygen	$K_{\mathrm{O_2}}/\mathrm{mol}\,\mathrm{m}^{-3}$	0.004
Charge transfer coefficient of anode	$\alpha/\mathrm{Dimensionless}$	0.051
Charge transfer coefficient of cathode	$\beta/\mathrm{Dimensionless}$	0.663

and variable selection. Firstly, the global sensitivity analysis based on variance can provide a deeper understanding of the interrelationship between parameters and power density. Secondly, the uncertainty analysis can optimize the uncertain parameters of the original model to make the system more robust. Finally, a neural network model based on data-driven and variable selection was established to simplify the model whereas optimizing the dimension of input variables.

A. SENSITIVITY ANALYSIS

The model proposed by Zeng *et al.* [25] assumes that only the valent cations M^+ transported through the membrane and M^+ ions are not involved in the cathodic reaction. During the modeling process, a number of parameters are obtained by experience or literatures. In addition, the empirical modeling of the electrochemical phenomena may render parameters such as the transfer coefficients in the Butler-Volmer equations to be uncertain. All of these lead to the great uncertainty of the proposed model, so it is necessary to analyze the uncertain parameters of the model before using the model to generate experimental data, and optimize the model properly. Sensitivity analysis is an important approach for obtaining higher prediction accuracy of model and measuring the precision of parameter estimates [26]–[28]. When a certain variable changes, SA can show the distribution of changes in other variables [29]. Sensitivity analysis is divided into two categories: Local sensitivity analysis (LSA) and Global sensitivity analysis. The LSA is an analysis of small changes in the input, whereas GSA is focuse on the interaction of multiple uncertain parameters on the whole system [30]. The advantage of local sensitivity analysis is the smaller amount of computation, but in order to obtain more accurate parameter sensitivity indicators, current research tend to use the global sensitivity analysis method [31].

1) GLOBAL SENSITIVITY ANALYSIS

The global sensitivity index based on variance decomposition analysis proposed by Sobol [32] in 1993 has become a critical foundation in the global sensitivity analysis method, and has been enriched by Homma and Saltelli [33]. It can deal with the nonlinear and non-monotonic models and can be represented by a function as follows:

$$Y = f(X) = f\left(X_1, X_2, \cdots X_p\right), \tag{16}$$

where Y represents the output values of the model, f stands for the model function and X_1, X_2, âĂęX_p are the factors that influence the outputs. Sobol suggested to expand the function as follows:

$$f\left(X_1, X_2, \cdots X_p\right) = f_0 + \sum_{i=1}^{p} f_i\left(X_i\right) + \sum_{i=1}^{p}\sum_{j=i+1}^{p} f_{ij}\left(X_i, X_j\right) + \cdots + f_{1,\cdots,p}\left(X_1, \cdots X_p\right). \tag{17}$$

If the input parameters are independent of each other and each term in this formula is set to zero average, which is square integrable, then f_0 is a constant. It's worth noting that this decomposition is unique.

The formula for calculating the total unconditional variance can be expressed as:

$$V(Y) = \int_{\Omega^p} f^2(X)\mathrm{d}X - f_0^2, \tag{18}$$

where Ω^p stands for the p-dimensional unit hyperspace. The partial variances can calculate from each of the terms in (19) as:

$$V_{i_1\cdots i_s} = \int_0^1 \cdots \int_0^1 f_{i_1\cdots i_s}^2 \left(X_{i_1}, \cdots, X_{i_s}\right) \mathrm{d}X_{i_1}, \cdots, \mathrm{d}X_{i_s}, \tag{19}$$

where $1 \le i_1 \le \cdots \le i_s \le p$ and $s = 1, \cdots, p$. Assuming that the parameters are orthogonal to each other, which result in (20).

$$V(Y) = \sum_{i=1}^{p} V_i + \sum_{i=1}^{p-1} \sum_{j=j+1}^{p} V_{ij} + \cdots + V_{1,\cdots,p}. \tag{20}$$

Through the above process, the contribution of the single parameter and the multiple parameters including this single parameter to the total output variance can be calculated. The sum of these contributions is represented by the total sensitivity indices:

$$\text{First order SI}: S_i = \frac{V_i}{V}, \tag{21}$$

$$\text{Second order SI}: S_{ij} = \frac{V_{ij}}{V}, \tag{22}$$

$$\text{Total SI}: S_{T_i} = S_i + \sum_{j \ne i} S_{ij} + \cdots. \tag{23}$$

The first order index, S_i, is a measure for the variance contribution of the parameter to the total model variance when it acts alone. S_{ij} denotes the effect of X_i with X_j. S_{T_i} stands for the main effect of X_i and all its interactions with the other parameters. In addition, S_{T_i} can also be obtained by (24),

$$S_{T_i} = 1 - \frac{V_{\sim i}}{V}, \tag{24}$$

where $V_{\sim i}$ stands for variance contribution except parameter X_i.

Due to the complexity of the MFC system, it is an extremely difficult process to calculate the variances by analytical integrals. To make it easier to calculate the sensitivity index, Monte Carlo (MC) integrals and Sobol' quasi-random sampling which can be found in the work of Saltelli *et al.* [34] was introduced into the calculation process.

The first order coefficient can be calculated as follows:

$$S_i = \frac{V_{X_i}\left(E_{X\sim i}\left(Y|X_i\right)\right)}{V(Y)}. \tag{25}$$

The total effect sensitivity analysis can be described as:

$$S_{T_i} = 1 - \frac{V_{X\sim i}\left(E_{X_i}\left(Y|X\sim i\right)\right)}{V(Y)} = \frac{E_{X\sim i}\left(V_{X_i}\left(Y|X\sim i\right)\right)}{V(Y)}, \tag{26}$$

where X_i represents a matrix of all factors, $X \sim i$ is a matrix of all factors except for the factor X_i, $V_{X_i}(\cdot)$and $E_{X_i}(\cdot)$ represent the variance and mean of argument $(\cdot)$ taken over X_i. $V_{X\sim i}(\cdot)$ and $E_{X\sim i}(\cdot)$ stand for variance and mean of argument $(\cdot)$ include all factors except for X_i, respectively.

To apply GSA, the details are described as follows:

1) Select the uncertainty parameters.
2) Set the range of parameters.
3) Within each parameter's range, sample points are generated by Sobol sampling.
4) Generate the matrices A, B, $A_B^{(i)}$ of each p parameter.

The calculation methods of $V_{X_i}(\cdot)$ and $E_{X\sim i}(\cdot)$ are as follows:

$$V_{X_i}\left(E_{X\sim i}\left(Y|X_i\right)\right) \approx \frac{1}{N}\sum_{j=1}^{N} f(B)_j \left(f\left(A_B^{(i)}\right)_j - f(A)_j\right), \tag{27}$$

$$E_{X\sim i}\left(V_{X_i}\left(Y|X\sim i\right)\right) \approx \frac{1}{2N}\sum_{j=1}^{N} \left(f(A)_j - f\left(A_B^{(i)}\right)_j\right)^2, \tag{28}$$

where A and B are design matrices of size $N \times p$, column i in matrix $A_B^{(i)}$ was selected from matrix B, and other $p-1$ columns was selected from matrix A. The settings of matrix A and B can be obtained from [34] and [35].

B. UNCERTAINTY PROPAGATION ANALYSIS

Sensitivity analysis are usually used in combination with and uncertainty analysis. The results of sensitivity analysis will be used as the basis for uncertainty analysis. Due to the complexity of microbial fuel cells, there are lots of uncertainty factors in the process of establishing microbial fuel cells and mathematical models. These uncertainty factors may be inherent or artificial. Different research fields and application objects have different classification of uncertainty. Generally, uncertainty factors can be divided into controllable factors and uncontrollable factors. Controllable factors include the geometric size of MFC model, manufacturing conditions, and so on. Uncontrollable factors include environmental factors, equipment depreciation, and so on. The Uncertainty facors in the MFCs system includes the inherent variability of the system, the inconsistency between model predicted and actual results, and the ambiguity exists in the problem description. The existence of uncertain parameters often leads to poor system robustness and difficulty in modeling. Therefore, evaluating the influence of uncertain parameters on MFC output has become one of the key steps in the system optimization and modeling. There are four main methods of uncertainty analysis: stochastic uncertainty analysis method, fuzzy uncertainty analysis method, hybrid uncertainty analysis method based on fuzzy stochastic theory and mixed uncertainty analysis method based on evidence theory. This paper focuses on the problem of stochastic uncertainty optimization. Uncertainty transfer means that the parameter uncertainty is transmitted to the output variable and the state variable through the internal action of the system.

Two mainstream methods can be used to quantitative calculation and qualitative description of uncertainty: Taylor expansion approximation and Random sampling simulation. Because the Taylor expansion approximation can not be applied to strong non-linear system, the random sampling simulation method was selected in this work.

The Monte Carlo stochastic simulation method is one of the most commonly used methods in the random sampling simulation method. This method can calculate the mean, variance and probability density of the system output. However, the traditional MC sampling method has the problem of low computational efficiency. Hence, this study uses a more uniform quasi-random number sequence instead of the original random number sequence to reduce the number of sample points and improve the computational efficiency and accuracy. Hammersley sequence sampling (HSS) is a new representative approximate random sampling technique which ensures the generated set of random numbers is representative and more in line with the real situation. The specific implementation process of HSS technique is described in [36], [37] as follows:

Before introducing the definition of HSS, we first introduce a basic operation, Radical Inversion:

$$i = \sum_{l=0}^{M-1} a_l(i)\, b^l, \tag{29}$$

$$\varphi_{b,C}(i) = \left(b^{-1} \cdots b^{-M}\right)\left[C\left(a_0(i) \cdots a_{M-1}(i)\right)^T\right], \tag{30}$$

where b is a positive integer, M is the number of digits, which allows for generating up to $N = b^M$ points. Firstly, any integer i is represented as base-b, the number $a_l(i)$ on each bit of the obtained number is arranged into a vector, and then multiplied by a generating matrix C to get a new vector. Finally, mirror this new vector to the right of the decimal point. $\varphi_{b,C}(i)$ is the result of radical inversion.

The Hammersley point set is generated when generator matrix C is a unit matrix and defined as:

$$X_i = \left(\frac{i}{N}, \varphi_{b_1}(i) \cdots \varphi_{b_{n-1}}(i)\right), \tag{31}$$

where $b_1 \cdots b_{n-1}$ are prime numbers, i is an index of sample points, and N stands for the number of points in the sample points.

The flow chart of uncertainty analysis in this paper is shown in Fig. 3. The details are given as follows:

1) The uncertain factor was used as a random variable, and the probability density function was set as normally distributed during the analysis.
2) HSS was used to generate random samples uniformly distributed in the interval [0, 1], and the Moro [38] method was used to convert the uniform random numbers into random samples obeying the normal distribution.
3) The degree of uncertainty of the inputs and output is measured by the coefficient of variation (COV). COV can reflect the discreteness of data under different data scales and units conditions. The larger of the COV, the greater of the uncertainty. The COV can be calculated as follows:

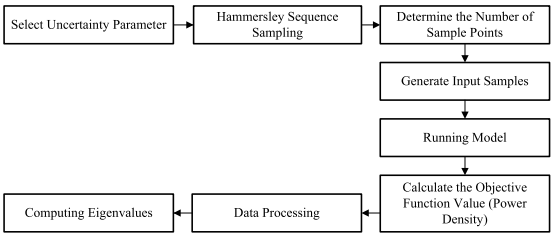

FIGURE 3. Flow diagram of MFC uncertainty analysis.

$$\mathrm{COV} = \frac{\sigma_\xi}{\mu_\xi}, \tag{32}$$

$$\mu_\xi \approx \bar{\xi} = \frac{1}{N}\sum_{i=1}^{N} \xi_i, \tag{33}$$

$$\sigma_\xi \approx s_\xi = \sqrt{\frac{1}{N-1}\sum_{i=1}^{N}\left(\xi_i - \bar{\xi}\right)}, \tag{34}$$

where ξ represents the input or output parameter, μ_ξ stands for the mean of the parameter, σ_ξ refers to the standard deviation of the parameter, and N represents the number of samples.

C. NEURAL NETWORK MODELING BASED ON DATA DRIVING AND VARIABLE SELECTION

Data-driven based neural network modeling is an efficient modeling method, which can greatly reduce the difficulty and workload of model building. By training a great amount of reaction precedents, Coley *et al.* [39] presented a supervised learning approach to predict the products of organic reactions. Ma *et al.* [40] chose the pH, temperature and voltage for correlation analysis and used radial basis function neural network and extreme learning machine to perform nonlinear system regression in the start-up stage of MFC. Based on neural network, Horiuchi *et al.* [41] proposed a simple modeling method for microbial dynamic behavior in a chemostat, which can be applied to the pH response in continuous anaerobic acidogenesis. Chen *et al.* [42] used cascade recurrent neural network model and modified genetic algorithm to optimized the fed-batch bioreactor. However, when the model contains a large number of input variables and the variables are not independent, the neural network modeling tends to have over-fitting phenomenon. This phenomenon will lead to the low accuracy of the established model and the long modeling time, which cannot be applied to the situation where the accuracy requirement is strict. The selection of independent variables can effectively reduce the dimension of independent variables and remove redundant independent variables. It can not only increase the accuracy of the model, but also simplify the MFCs model, making it more versatile. In recent years, the most popular methods of

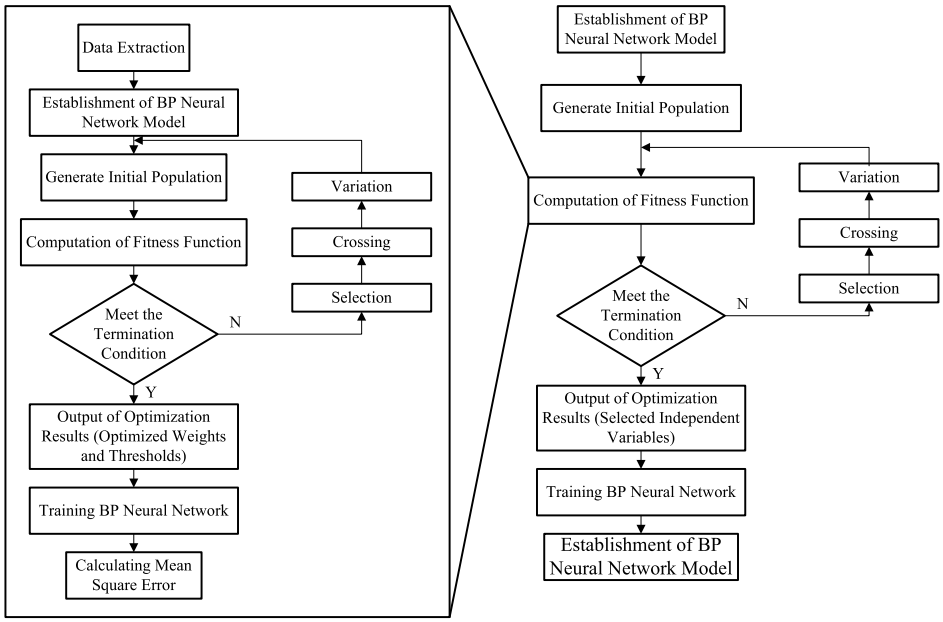

FIGURE 4. Flow diagram of neural network modeling system based on data driven and independent variable selection.

variable selection include multivariate regression, correlation analysis, principal component analysis, partial least squares and genetic algorithms. Due to the genetic algorithm has the characteristics of global optimization and low computational complexity, this paper chooses genetic algorithm as the method of independent variable screening. Firstly, the neural network is constructed by HSS and data-driven method, and then the genetic algorithm was used to obtain the optimal input variables.

Using genetic algorithms for optimization calculations, the solution space needs to be mapped to the coding space, and each code corresponds to a solution to the problem. After continuous iteration, the most representative input independent variables are selected to participate in the modeling. Since the number of independent variables used for modeling in each genetic algorithm iteration is different, the optimal weight and threshold of each BP neural network are also different. In order to solve this problem, we nest a genetic algorithm again, and select the optimal weight and threshold in the process of variable selection fitness function calculation to solve the above problems, so that the result of variable selection is more accurate. The flow of neural network modeling system based on data driven and independent variable selection is shown in the Fig. 4.

The fitness function of the independent variable screening based on genetic algorithm is the reciprocal of the squared sum of the error between the predicted value and the true value of the test set data is described as (35):

$$f(X) = \frac{1}{SE} = \frac{1}{sse(\overline{T} - T)} = \frac{1}{\sum_{i=1}^{n} \left(\overline{t_i} - t_i\right)^2}, \quad (35)$$

TABLE 2. Range of selected uncertain parameters for the sensitivity analysis.

Symbol/ Unit	The initial value	Lower limit	Upper limit
$k_1^0/\mathrm{mol\,m^{-2}\,h^{-1}}$	0.207	0.1656	0.2484
$K_{\mathrm{AC}}/\mathrm{mol\,m^{-3}}$	0.592	0.4736	0.7104
$k_2^0/\mathrm{m^{12}\,mol^{-4}\,h^{-1}}$	0.00003288	0.0000263	0.000039456
α/Dimensionless	0.051	0.0408	0.0612
β/Dimensionless	0.663	0.5304	0.7956
$K_{\mathrm{O_2}}/\mathrm{mol\,m^{-3}}$	0.004	0.0032	0.0048

where $\overline{T} = \left\{\overline{t_1}, \overline{t_2}, \cdots, \overline{t_n}\right\}$ is the predicted value of the test set, $T = \{t_1, t_2, \cdots, t_n\}$ represents the true value of the test set, and n is the number of samples in the test set.

IV. RESULTS AND DISCUSSION

A. GLOBAL SENSITIVITY ANALYSIS OF MFC MODEL

This section mainly introduces how to apply GSA to MFCs simulation model, and evaluates the influence of uncertain parameters in the model on the CSTR system. The uncertain parameters includes the forward rate constant of anodic reaction at standard conditions (k_1^0), the half velocity rate constant for acetate (K_{AC}), the forward rate constant of cathodic reaction at standard conditions (k_2^0), the anodic charge transfer coefficient (α), the cathodic charge transfer coefficient (β), and half velocity rate constant for dissolved oxygen ($K_{\mathrm{O_2}}$).

For this research, a sample size of 5000 was used to calculate the first order and total sensitivity index. Sobol sequences were generated at different ranges for all uncertain parameters. In the process of model operation, the center value and range of uncertain parameters are given in Table 2. The values of other parameters are obtained from Table 1.

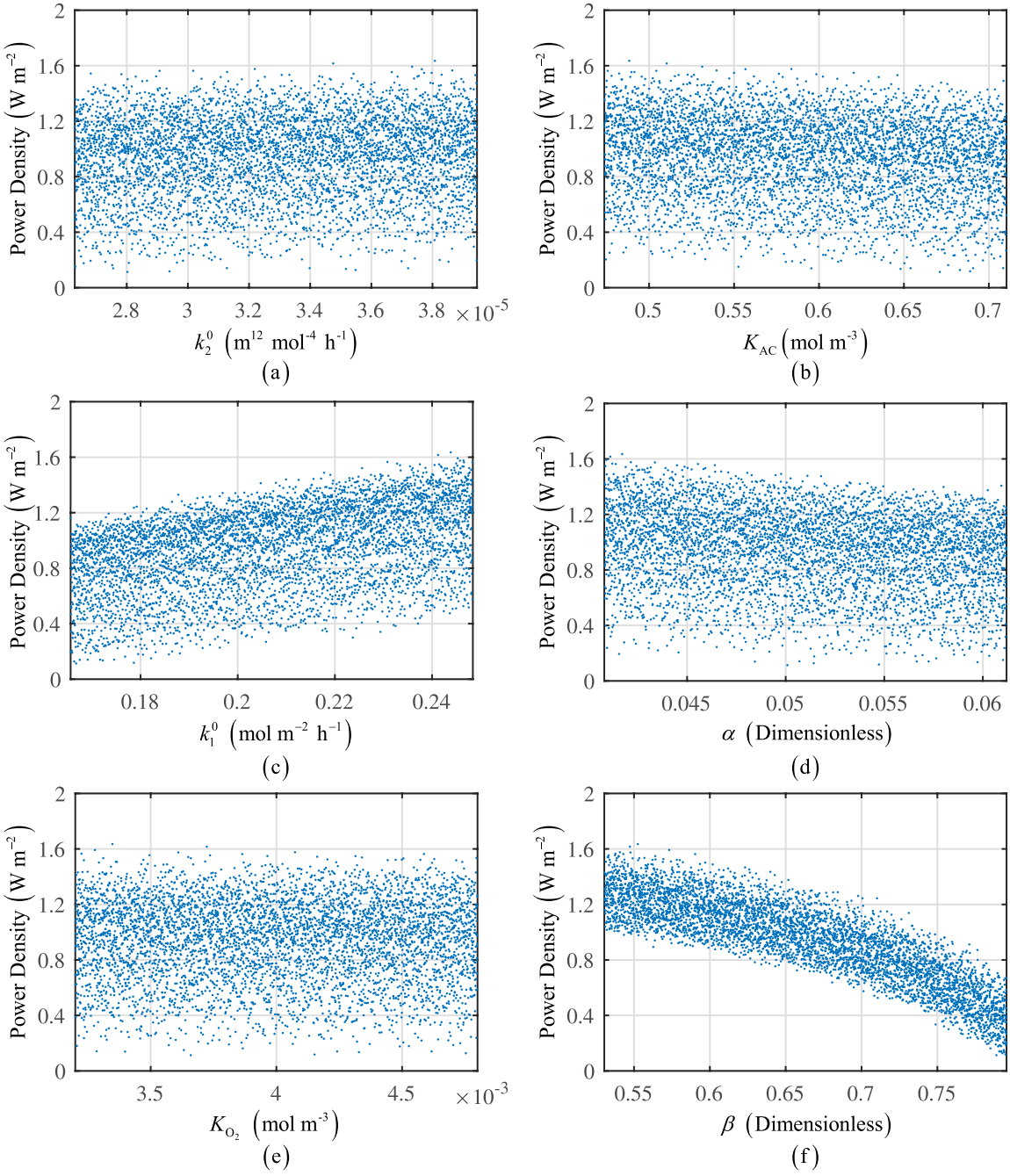

FIGURE 5. Dependence of power density on (a) forward rate constant of cathode reaction at standard conditions, (b) half velocity rate constant for acetate, (c) forward rate constant of anodic reaction at standard conditions, (d) anodic charge transfer coefficient (e) half velocity rate constant for dissolved oxygen and (f) charge transfer coefficient of cathode.

The scatter diagram of the MFC power density versus the forward rate constant of cathodic reaction and the half velocity rate constant for acetate are shown in Fig. 5(a) and Fig. 5(b). From these graphs, we can draw the conclusion that these two parameters show a weak linear pattern. The power density slightly decrease as K_{AC} increase, and increase as k_2^0 increase. The scatter plots, shown in Fig. 5(c) and Fig. 5(d), exhibit obvious strong linear relationship, which indicate the power density is sensitive to the forward rate constant of anodic reaction and the anodic charge transfer coefficient. The power density increased by 0.5 W m^{-2} during the change of k_1^0 from 0.1656 mol m^{-2} h^{-2} to 0.248 mol m^{-2} h^{-2}. On the contrary, the power density decrease linearly with the change of α from 0.0408 to 0.0612. According to scatter plots Fig. 5(e), the interaction between K_{O_2} and power density is insignificant, and the change of K_{O_2} can hardly affect the power density. It also shows that the uncertainty of K_{O_2} has less influence on the system, and the influence of changes

TABLE 3. First order effects and total effects of the uncertain parameters.

Symbol/Unit	First order effect	Total effect
$k_1^0/\mathrm{mol\,m^{-2}\,h^{-1}}$	0.1779	0.1781
$K_{\mathrm{AC}}/\mathrm{mol\,m^{-3}}$	0.016	0.0161
$k_2^0/\mathrm{m^{12}\,mol^{-4}\,h^{-1}}$	0.0032	0.0046
α/Dimensionless	0.0346	0.0376
β/Dimensionless	0.7653	0.7666
$K_{\mathrm{O_2}}/\mathrm{mol\,m^{-3}}$	1.0961×10^{-6}	1.1117×10^{-6}

on half velocity rate constant for dissolved oxygen can be neglected in the process of modeling. It can be seen from Fig. 5(f) that the power density has a non-linear relationship with β. In the course of β changes in the range of 0.5304 to 0.7956, the power density of MFC decreases slowly first and then decreases rapidly. This indicates that changes in the uncertain parameter β during the experiment should be focused.

The first-order sensitivity coefficient based on the Sobol' method reflects the influence extent of the variable on the power density when the variable acts alone. The total sensitivity reflects the influence of the parameter on the function value after considering the cross-action of variables. The higher the sensitivity of the uncertain parameter, the larger the first-order sensitivity coefficient. The first-order sensitivity coefficient and the total sensitivity coefficient of the MFC uncertain parameters can be calculated by (25) and (26) as listed in Table 3. As the data displayed in table, the order of first-order sensitivity coefficient for the uncertain parameters is β, k_1^0, α, K_{AC}, k_2^0, and $K_{\mathrm{O_2}}$ which is the same as total sensitivity. The relationship between uncertain parameters can be seen more intuitively by the histogram generated in Table 3 as shown in Fig. 6. As we can see from Fig. 6 that the first-order sensitivity coefficient and the total sensitivity coefficient of β are significantly higher than other parameters, and the value of $K_{\mathrm{O_2}}$ is close to zero, which is consistent with our previous analysis. It is worth noting that the first-order sensitivity of almost all parameters is very close to its total sensitivity, which indicates that the interaction between these six uncertain parameters is minimal. In the case where multiple uncertain parameters change simultaneously, that is, under more complicated experimental conditions, the output power is only slightly different from the condition of a single parameter change.

B. UNCERTAINTY ANALYSIS OF MFC MODEL

Through the global sensitivity analysis, it can be concluded that five of the six uncertain parameters have obvious influence on the power density, and the interaction between the parameters is minimal. In this section, five parameters k_1^0, K_{AC}, k_2^0, α, and β, which have a significant influence on power density, will be selected for further analysis. In the uncertainty analysis process, the mean values of these five parameters are selected according to Table 2, and the coefficient of variation ranges from 0 to 0.1. In addition,

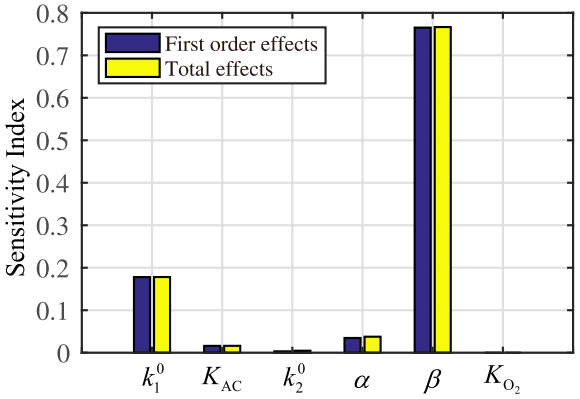

FIGURE 6. Sensitivity indices for the first order effects and total effects of the uncertainty parametersc.

the remaining parameters are determined according to the data in Table 1.

The number of sampling points has a great impact on the running time and accuracy of the model. If the number of sampling points is too small, the calculation accuracy will be reduced. However, too many sampling points will lead to lengthy computation time. Hence, the determination of the number of sampling points is the premise to solve the problem of uncertainty analysis. In the calculation process, the COV for all uncertain parameters is set equal to 0.05. Fig. 7(a) and Fig. 7(b) show the variation of the mean and standard deviation as the number of sampling points increases. As we can see from the figure that the mean and standard deviation of power density gradually converge with the increase of the number of sampling points, and the number of samples is stable at 2000. As a result, the number of sampling points in the uncertainty analysis of this study was set to 2000.

Different uncertain parameter has different effects on the COV of power density. In the uncertainty analysis, the mean of a certain uncertain factor is divided into three grades whereas others factor's standard values are settled as listed in Table 2, and the current density is taken as $i_{\mathrm{cell}} = 2\,\mathrm{A\,m^{-2}}$. The relationship between input parameters and output is shown in Fig. 8.

It can be seen in Fig. 8(a) that as the COV of k_1^0 increases, the coefficient of variation of the power density increases linearly. In the case of the same COV of power density, an increase in the mean of k_1^0 results in a lower COV of power density, which is more pronounced when COV of k_1^0 is higher. In Fig. 8(b), when the mean values of K_{AC} are set as 0.592 and 0.4736, the curve is still linearly increasing, but when it comes to 0.7104, the curve becomes nonlinear. In the case of the same coefficient of variation, an increase in the mean of K_{AC} results in a higher COV of power density. The same phenomenon is more obvious when the COV of K_{AC} is larger. The case of k_2^0 as given in Fig. 8(c) is completely opposite to k_1^0. The larger the mean value of k_2^0, the larger the COV of power density. In the case of three different values of mean of k_2^0, the COV of power density has linear relationship with the COV of k_2^0. As it shown in Fig. 8(d), the uncertainty

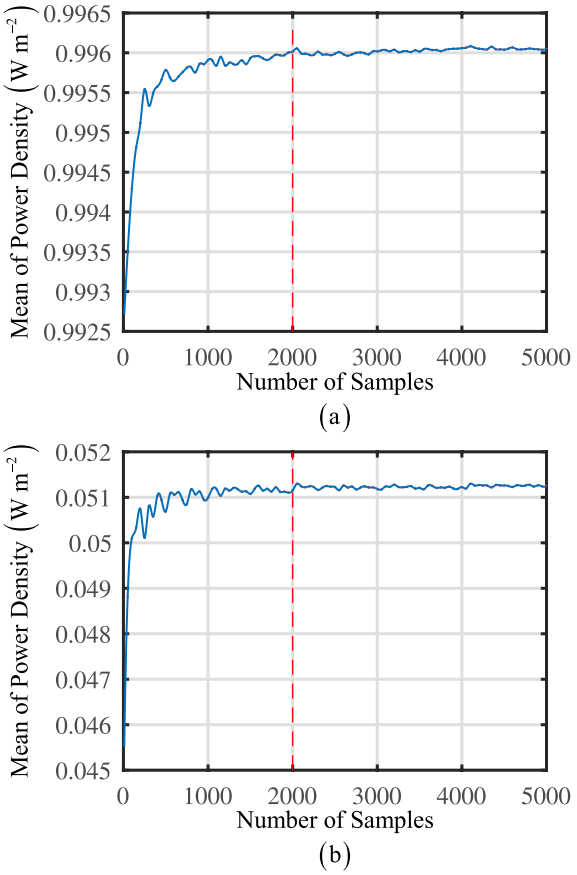

FIGURE 7. Diagram of the relation between (a) mean of power density and number of samples and (b) standard deviation of power density and number of samples.

analysis has performed on α. When the mean values of α are equal to 0.0408 and 0.0501, the curves appear to overlap. This illustrates when the mean value of α is lower, the mean of α changes will no longer be a major factor affecting COV of power density. At the same time, the COV of power density will be lower under the condition of higher α average. As we can see from Fig. 8(e), when the mean value of β is 0.7956, the COV of β and COV of power density exhibit an obviously nonlinear relationship, and with the increase of the coefficient of variation of β, the growth rate of COV of β is faster and faster, until the final result is far greater than the average value of β is 0.5304 and 0.663. At the same time, when the mean value of β equal to 0.5304 and 0.663, the nonlinearity and difference of the curve are very small. This indicates that the mean of β will have a great influence on COV of power density, the experimenter should precisely control the value of β in the course of the experiment to ensure a lower COV of power density.

In order to further explore the above phenomenon, we conducted further analysis to fix the coefficient of variation of all uncertain factors to 0.05, and explored the effect of the change in the mean value of the uncertain parameter on the power density. It can be seen from Fig. 9(a) that as the mean value of the parameter k_1^0 increases, the standard deviation of the power density changes in a wave shape, and the lowest point is at $k_1^0 = 0.226$. An increase in the mean of parameter K_{AC} results in an increase in the standard deviation of the power density and a decrease in the mean of the power density, which is the same as the case of Fig. 9(e). The difference is that the non-linear relationship between the mean of parameter and the mean or standard deviation of power density in Fig. 9(e) is much larger than that in Fig. 9(a). In Fig. 9(c) and Fig. 9(d), it can be seen that the change of the standard deviation of the power density is the same as the change trend of the mean value, which is an upward trend during the change of the parameter k_2^0, and a downward trend during the change of the parameter α.

TABLE 4. Range of input parameters for the neural network modeling.

Symbol/Unit	Lower limit	Upper limit
$Q_{\mathrm{a}}/\mathrm{m}^3\,\mathrm{h}^{-1}$	1.8×10^{-5}	2.7×10^{-5}
$Q_{\mathrm{c}}/\mathrm{m}^3\,\mathrm{h}^{-1}$	0.888×10^{-3}	1.332×10^{-3}
$i_{\mathrm{cell}}/\mathrm{A}\,\mathrm{m}^{-2}$	2	10
$C_{\mathrm{AC}}^{\mathrm{in}}/\mathrm{mol}\,\mathrm{m}^{-3}$	1.248	1.872
$C_{\mathrm{CO_2}}^{\mathrm{in}}/\mathrm{mol}\,\mathrm{m}^{-3}$	0	0.2
$C_{\mathrm{H}}^{\mathrm{in}}/\mathrm{mol}\,\mathrm{m}^{-3}$	0	0.2
$X^{\mathrm{in}}/\mathrm{mol}\,\mathrm{m}^{-3}$	0	0.2
$C_{\mathrm{O_2}}^{\mathrm{in}}/\mathrm{mol}\,\mathrm{m}^{-3}$	0.25	0.375
$C_{\mathrm{OH}}^{\mathrm{in}}/\mathrm{mol}\,\mathrm{m}^{-3}$	0	0.2
$C_{\mathrm{M}}^{in}/\mathrm{mol}\,\mathrm{m}^{-3}$	0	0.2

In summary, the existence of uncertain parameters can lead to poor robustness of neural network modeling. In this paper, the robustness of the model is improved by appropriately changing the value of the uncertain parameter, and it provides a basis for neural network modeling. The criterion for the optimization of uncertain parameters is to find the point with the largest mean value of power density under the condition that the coefficient of variation and the standard deviation of the model output are the smallest. The value of the uncertain parameter after optimization were set as $k_1^0 = 0.2226$, $K_{\mathrm{AC}} = 0.4736$, $k_2^0 = 0.0000263$, $\alpha = 0.0612$, $\beta = 0.5304$.

C. VARIABLE SELECTION AND NEURAL NETWORK MODELING OF MFC

BP neural network is a typical multi-layer feedforward neural network. In the process of network operation, the signal is forwarded and the error is reversed. Through the above sensitivity analysis and uncertainty analysis, we optimize the value of the uncertain parameter to make the model more robust. Excessively high input parameter dimensions can greatly increase the complexity of the model and make the model less versatile. The method of reducing the dimension of the independent variables reduces the coupling between the independent variables in the original model, so that the model fitted by the BP neural network is more universal in the case of ensuring the modeling accuracy.

Firstly, the experimental data is generated by simulating the model introduced in Section 2. Among them, the uncertain parameters were set as optimized result, and the lower and upper limits of the input parameters values are shown in Table 4. The power density of the MFC model is referred to

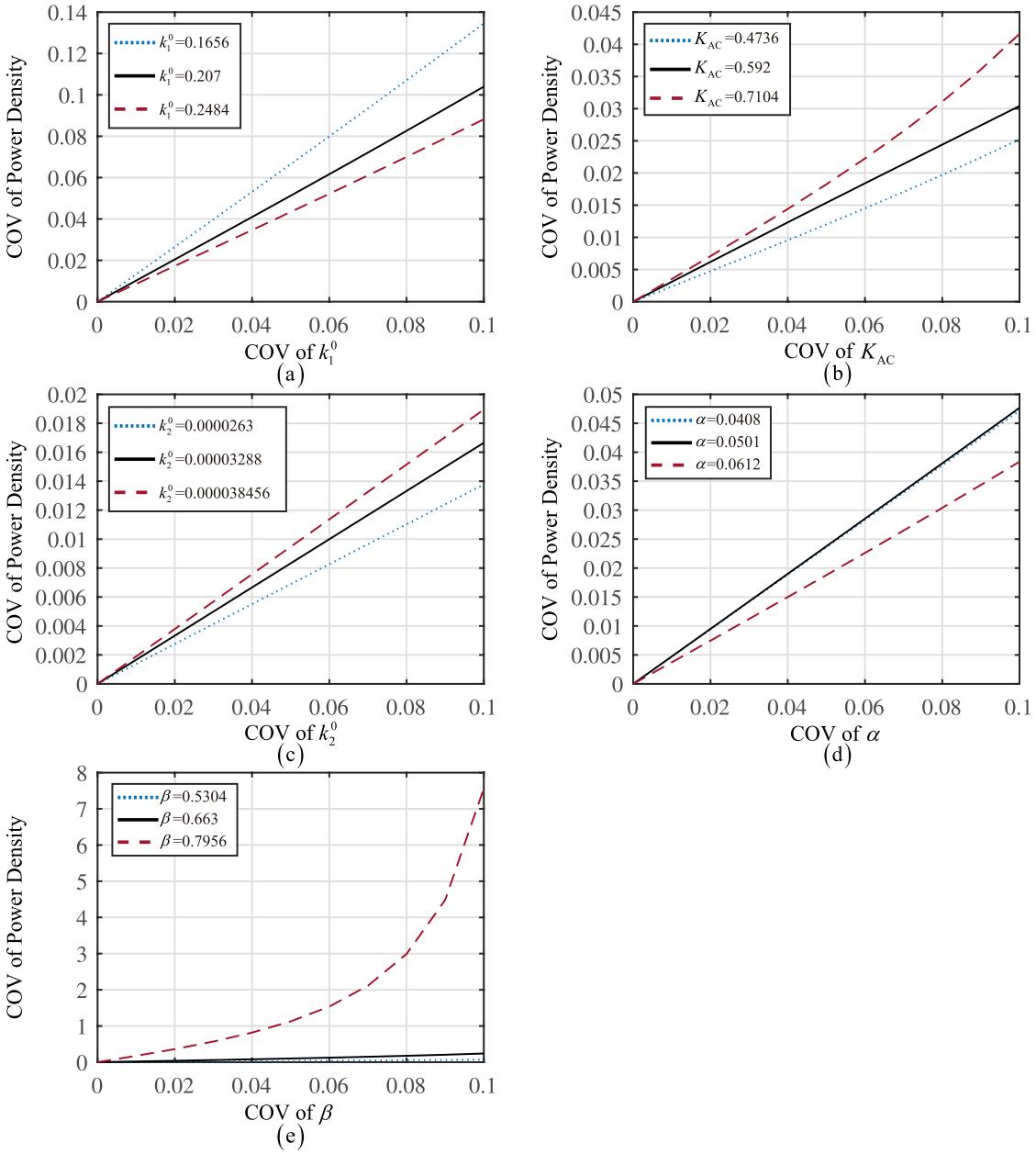

FIGURE 8. Dependence of COV of power density on COV of (a) forward rate constant of anode reaction at standard condition, (b) half velocity rate constant for acetate, (c) forward rate constant of cathode reaction at standard condition, (d) charge transfer coefficient of anode and (e) charge transfer coefficient of cathode.

the true value in subsequent analysis, and assuming that the values of all the operating parameters are evenly distributed in their corresponding upper and lower limits. The data of all training sets and test sets in BP neural network are acquired by HSS method through simulating the initial MFC model.

The 4500 data represented by 10 input parameters were used in neural network modeling, and 500 sets of data were used for prediction results as shown in Fig. 10(a). It can be seen from the error graph that the prediction accuracy of the neural network model has reached the level of two decimal places. However, there are several sample points in the graph where the predicted values show a relatively large deviation. This can not meet the requirement of MFCs for power density prediction accuracy. The mean square error predicted by the calculation of 10 parameters participating in the prediction is 0.00014982.

In order to improve the prediction accuracy and reduce the complexity of the model, the method described in Section 3.3 was used to filter the independent variables. After the genetic algorithm optimization, the selected set of independent variables are Q_a, i_{cell}, C_{AC}^{in}, C_H^{in}, and X^{in}. Obviously, after genetic algorithm optimization and

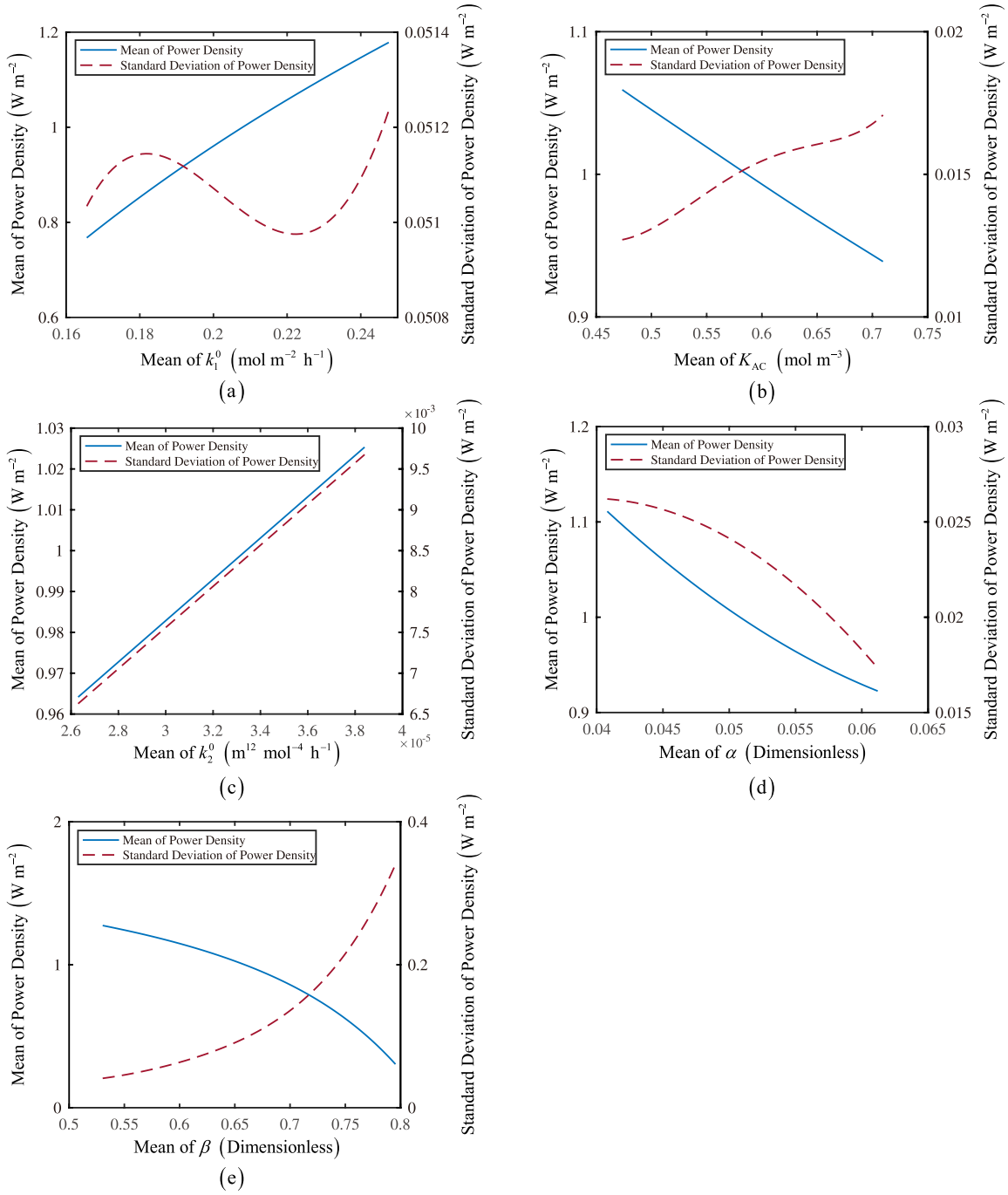

FIGURE 9. Dependence of mean and standard deviation of power density on mean of (a) forward rate constant of anode reaction at standard condition, (b) half velocity rate constant for acetate, (c) forward rate constant of cathode reaction at standard condition, (d) charge transfer coefficient of anode and (e) charge transfer coefficient of cathode.

screening, the number of input independent variables participating in the modeling is half of the total numbers, and the mean square error is reduced to 0.00012547. At the same time, the modeling time is reduced from 12.5156 seconds to 2.8125 seconds. Fig. 10(b) gives the results of prediction error after variable selection. The results show that the error of model prediction is greatly reduced, and there is no sample point with excessive prediction error. The prediction error of the sample points is approximately between −0.02 and 0.04. It is indicated that the proposed method can effectively improve the prediction accuracy of BP neural model and significantly reduce the complexity of MFC mathematical model, which has practical significance. In summary, the neural network model is an alternative method to capture the nonlinear relationship between the input parameters and power density of MFCs. It can simplify the model

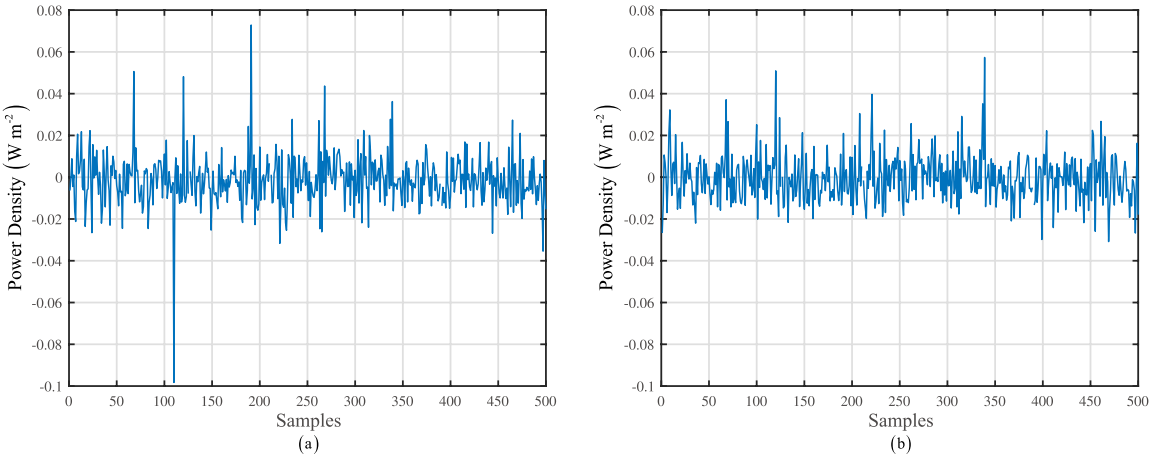

FIGURE 10. Diagram of the absolute error between expected output and predictive output: (a) before variable selection and (b) after variable selection.

of complex differential equation sufficiently to guide the experiment.

V. CONCLUSION

In this paper, the framework of microbial fuel cell model analysis and neural network modeling is discussed in detail. Firstly, the global sensitivity analysis and uncertainty analysis of the model are carried out to explore the influence of the uncertainty parameters on the system and optimize the value of the uncertainty parameters. The analysis results show that the cathodic charge transfer coefficient has the greatest effect on the power density, whereas the half velocity rate constant for dissolved oxygen has almost no effect on the results. Compared to the case where the uncertainty parameter acts alone, the interaction between the uncertain parameters has less impact on the system. The uncertain parameters were optimized by uncertainty analysis to make the MFC mathematical model more applicable under uncertainty conditions. Secondly, the combination of genetic algorithm-based variable selection and neural network can reduce the complexity of the model, improve the accuracy of the neural network modeling, and provide a new direction for model simplification. Compared with the original model, the number of input parameters in the neural network model are reduced from 10 to 5. The framework presented in this paper can also be used as an optimization for other types of fuel cell analysis.

ACKNOWLEDGMENT

The authors are grateful to the IEEE Fellow, professor of the Chinese university of Hong Kong, P. Yum, for his suggestions on this article.

REFERENCES

[1] I. Lee, G. Kim, S. Bang, A. Wolfe, R. Bell, S. Jeong, Y. Kim, J. Kagan, M. Arias-Thode, B. Chadwick, D. Sylvester, D. Blaauw, and Y. Lee, "System-on-mud: Ultra-low power oceanic sensing platform powered by small-scale benthic microbial fuel cells," *IEEE Trans. Circuits Syst. I, Reg. Papers*, vol. 62, no. 4, pp. 1126–1135, Apr. 2015.

[2] I. A. Anderson, I. A. Ieropoulos, T. McKay, B. O'Brien, and C. Melhuish, "Power for robotic artificial muscles," *IEEE/ASME Trans. Mechatronics*, vol. 16, no. 1, pp. 107–111, Feb. 2010.

[3] P. R. Bandyopadhyay, D. P. Thivierge, F. M. McNeilly, and A. Fredette, "An electronic circuit for trickle charge harvesting from littoral microbial fuel cells," *IEEE J. Ocean. Eng.*, vol. 38, no. 1, pp. 32–42, Jan. 2013.

[4] K. Rabaey, N. Boon, M. Höfte, and W. Verstraete, "Microbial phenazine production enhances electron transfer in biofuel cells," *Environ. Sci. Technol.*, vol. 39, no. 9, pp. 3401–3408, 2005.

[5] G. Reguera, K. P. Nevin, J. S. Nicoll, S. F. Covalla, T. L. Woodard, and D. R. Lovley, "Biofilm and nanowire production leads to increased current in *Geobacter sulfurreducens* fuel cells," *Appl. Environ. Microbiol.*, vol. 72, no. 11, pp. 7345–7348, 2006.

[6] C. I. Torres, A. K. Marcus, H.-S. Lee, P. Parameswaran, R. Krajmalnik-Brown, and B. E. Rittmann, "A kinetic perspective on extracellular electron transfer by anode-respiring bacteria," *FEMS Microbiol. Rev.*, vol. 34, no. 1, pp. 3–17, 2010.

[7] C. A. Pham, S. J. Jung, N. T. Phung, J. Lee, I. S. Chang, B. H. Kim, H. Yi, and J. Chun, "A novel electrochemically active and Fe(III)-reducing bacterium phylogenetically related to *Aeromonas hydrophila*, isolated from a microbial fuel cell," *FEMS Microbiol. Lett.*, vol. 223, no. 1, pp. 129–134, 2003.

[8] B. E. Logan, C. Murano, K. Scott, N. D. Gray, and I. M. Head, "Electricity generation from cysteine in a microbial fuel cell," *Water Res.*, vol. 39, no. 5, pp. 942–952, 2005.

[9] Y. Liu, H. Xu, J. Han, C. Chang, and B. Chen, "Influence of substrate concentration, electrode space and ionic strength on microbial fuel cell," *Environ. Sci. Technol., China*, vol. 34, no. 9, pp. 157–161, 2011.

[10] G. S. Jadhav and M. M. Ghangrekar, "Performance of microbial fuel cell subjected to variation in pH, temperature, external load and substrate concentration," *Bioresource Technol.*, vol. 100, no. 2, pp. 717–723, 2009.

[11] A. G. del Campo, J. Lobato, P. Cañizares, M. A. Rodrigo, and F. F. J. Morales, "Short-term effects of temperature and COD in a microbial fuel cell," *Appl. Energy*, vol. 101, pp. 213–217, Jan. 2013.

[12] S. Puig, M. Serra, M. Coma, M. Cabré, M. D. Balaguer, and J. Colprim, "Effect of pH on nutrient dynamics and electricity production using microbial fuel cells," *Bioresource Technol.*, vol. 101, no. 24, pp. 9594–9599, 2010.

[13] J.-Y. Nam, H.-W. Kim, K.-H. Lim, H.-S. Shin, and B. E. Logan, "Variation of power generation at different buffer types and conductivities in single chamber microbial fuel cells," *Biosensors Bioelectron.*, vol. 25, no. 5, pp. 1155–1159, 2010.

[14] H.-W. Kim, J.-Y. Nam, and H.-S. Shin, "Ammonia inhibition and microbial adaptation in continuous single-chamber microbial fuel cells," *J. Power Sources*, vol. 196, no. 15, pp. 6210–6213, 2011.

[15] K. Raman and J. C.-W. Lan, "Performance and kinetic study of photo microbial fuel cells (PMFCs) with different electrode distances," *Appl. Energy*, vol. 100, pp. 100–105, Dec. 2012.

[16] Y. Zou, C. Xiang, L. Yang, L.-X. Sun, F. Xu, and Z. Cao, "A mediatorless microbial fuel cell using polypyrrole coated carbon nanotubes composite as anode material," *Int. J. Hydrogen Energy*, vol. 33, no. 18, pp. 4856–4862, 2008.
[17] Z. Ren, L. M. Steinberg, and J. M. Regan, "Electricity production and microbial biofilm characterization in cellulose-fed microbial fuel cells," *Water Sci. Technol.*, vol. 58, no. 3, pp. 617–622, 2008.
[18] H. Liu, S. Cheng, and B. E. Logan, "Power generation in fed-batch microbial fuel cells as a function of ionic strength, temperature, and reactor configuration," *Environ. Sci. Technol.*, vol. 39, no. 14, pp. 5488–5493, 2005.
[19] L. Qiang, L. J. Yuan, and Q. Ding, "Influence of buffer solutions on the performance of microbial fuel cell electricity generation," *Huan Jing xue= Huanjing Kexue*, vol. 32, no. 5, pp. 1524–1528, 2011.
[20] V. M. Ortiz-Martínez, M. J. Salar-García, A. P. de los Ríos, F. J. Hernández-Fernández, J. A. Egea, and L. J. Lozano, "Developments in microbial fuel cell modeling," *Chem. Eng. J.*, vol. 271, pp. 50–60, Jul. 2015.
[21] C. Picioreanu, I. M. Head, K. P. Katuri, M. C. M. van Loosdrecht, and K. Scott, "A computational model for biofilm-based microbial fuel cells," *Water Res.*, vol. 41, no. 13, pp. 2921–2940, 2007.
[22] M. K. Alavijeh, M. M. Mardanpour, and S. Yaghmaei, "A generalized model for complex wastewater treatment with simultaneous bioenergy production using the microbial electrochemical cell," *Electrochim. Acta*, vol. 167, pp. 84–96, Jun. 2015.
[23] K. P. Katuri and K. Scott, "On the dynamic response of the anode in microbial fuel cells," *Enzyme Microbial Technol.*, vol. 48, nos. 4–5, pp. 351–358, 2011.
[24] S. Ou, Y. Zhao, D. S. Aaron, J. M. Regan, and M. M. Mench, "Modeling and validation of single-chamber microbial fuel cell cathode biofilm growth and response to oxidant gas composition," *J. Power Sources*, vol. 328, pp. 385–396, Oct. 2016.
[25] Y. Zeng, Y. F. Choo, B.-H. Kim, and P. Wu, "Modelling and simulation of two-chamber microbial fuel cell," *J. Power Sources*, vol. 195, no. 1, pp. 79–89, 2010.
[26] A. Saltelli, S. Tarantola, F. Campolongo, and M. Ratto, *Sensitivity Analysis in Practice: A Guide to Assessing Scientific Models*. Chichester, U.K.: Wiley, 2004.
[27] J. Norton, "An introduction to sensitivity assessment of simulation models," *Environ. Model. Softw.*, vol. 69, pp. 166–174, Jul. 2015.
[28] X. Song, J. Zhang, C. Zhan, Y. Xuan, M. Ye, and C. Xu, "Global sensitivity analysis in hydrological modeling: Review of concepts, methods, theoretical framework, and applications," *J. Hydrol.*, vol. 523, pp. 739–757, Apr. 2015.
[29] W. E. Thogmartin, "Sensitivity analysis of North American bird population estimates," *Ecol. Model.*, vol. 221, no. 2, pp. 173–177, 2010.
[30] I. Dimov and R. Georgieva, "Monte Carlo algorithms for evaluating Sobol' sensitivity indices," *Math. Comput. Simul.*, vol. 81, no. 3, pp. 506–514, 2010.
[31] A. van Griensven, T. Meixner, S. Grunwald, T. Bishop, M. Diluzio, and R. Srinivasan, "A global sensitivity analysis tool for the parameters of multi-variable catchment models," *J. Hydrol.*, vol. 324, nos. 1–4, pp. 10–23, Jun. 2006.
[32] I. M. Sobol, "Sensitivity estimates for nonlinear mathematical models," *Math. Model. Comput. Experim.*, vol. 1, no. 4, pp. 407–414, 1990.
[33] T. Homma and A. Saltelli, "Importance measures in global sensitivity analysis of nonlinear models," *Rel. Eng. Syst. Saf.*, vol. 52, no. 1, pp. 1–17, 1996.
[34] A. Saltelli, P. Annoni, I. Azzini, F. Campolongo, M. Ratto, and S. Tarantola, "Variance based sensitivity analysis of model output. Design and estimator for the total sensitivity index," *Comput. Phys. Commun.*, vol. 181, no. 2, pp. 259–270, Feb. 2010.
[35] I. M. Sobol and B. V. Shukman, "Random and quasirandom sequences: Numerical estimates of uniformity of distribution," *Math. Comput. Model.*, vol. 18, no. 8, pp. 39–45, 1993.
[36] J. R. Kalagnanam and U. M. Diwekar, "An efficient sampling technique for off-line quality control," *Technometrics*, vol. 39, no. 3, pp. 308–319, 1997.
[37] U. M. Diwekar and J. R. Kalagnanam, "Efficient sampling technique for optimization under uncertainty," *AIChE J.*, vol. 43, no. 2, pp. 440–447, Feb. 1997.
[38] J. D. Beasley and S. G. Springer, "The percentage points of the normal distribution," *J. Roy. Stat. Soc. C, Appl. Statist.*, vol. 26, no. 1, pp. 118–121, 1977.
[39] C. W. Coley, W. Jin, L. Rogers, T. F. Jamison, T. S. Jaakkola, W. H. Green, R. Barzilay, and K. F. Jensen, "A graph-convolutional neural network model for the prediction of chemical reactivity," *Chem. Sci.*, vol. 10, no. 2, pp. 370–377, 2019.
[40] F. Ma, Y. Yin, and M. Li, "Start-up process modelling of sediment microbial fuel cells based on data driven," *Math. Problems Eng.*, vol. 2019, Jan. 2019, Art. no. 7403732.
[41] J.-I. Horiuchi, S. Kikuchi, M. Kobayashi, T. Kanno, and T. Shimizu, "Modeling of pH response in continuous anaerobic acidogenesis by an artificial neural network," *Biochem. Eng. J.*, vol. 9, no. 3, pp. 199–204, 2001.
[42] L. Chen, S. K. Nguang, X. D. Chen, and X. M. Li, "Modelling and optimization of fed-batch fermentation processes using dynamic neural networks and genetic algorithms," *Biochem. Eng. J.*, vol. 22, no. 1, pp. 51–61, 2004.

FENGYING MA received the B.Eng. degree in automation and the M.S. degree in control theory and control engineering from the Shandong University of Science and Technology, Jinan, China, in 1996 and 1999, respectively, and the Ph.D. degree in communications and information systems from the China University of Mining and Technology, Beijing, China, in 2009. In 1999, she joined the School of Electrical Engineering and Automation, Qilu University of Technology, where she is currently a Professor. Her research interests include machine learning, computer networks, and wireless communications.

YANKAI YIN received the B.Eng. degree in electrical engineering and automation from the Qilu University of Technology, Jinan, China, in 2017, where he is currently pursuing the M.S. degree in control science and technology with the School of Electrical Engineering and Automation. His research interests include drone communication, fault diagnosis, and mathematical modeling.

SHAOPENG PANG received the Ph.D. degree in control theory and control engineering from Beihang University. He has published nine SCI-indexed journal articles as the first author or correspondent author. His research interests include complex systems, machine learning, and data mining.

JIAXUN LIU was born in Rizhao, Shandong, China. He received the B.Eng. degree from the College of Electrical Engineering and Automation, Qilu University of Technology (Shandong Academy of Sciences), where he is currently pursuing the master's degree. His research interests include nonlinear dynamics and the application of nonlinear systems.

WEI CHEN received the B.Eng. degree in medical imaging and the M.S. degree in paleontology and stratigraphy from the China University of Mining and Technology, Xuzhou, China, in 2001 and 2005, respectively, and the Ph.D. degree in communications and information systems from the China University of Mining and Technology, Beijing, China, in 2008. In 2008, he joined the School of Computer Science and Technology, China University of Mining and Technology, where he is currently a Professor. His research interests include machine learning, image processing, and computer networks. He is a member of the ACM and EAI.